Adaptive Mho Characteristic-Based Distance Protection for Lines Emanating From Photovoltaic Power Plants Under Unbalanced Faults

Yingyu Liang, *Member, IEEE*, Wulin Li, and Wenting Zha

***Abstract*—The exclusive fault characteristics of photovoltaic (PV) power plants and the existence of fault resistance cause a high probability of failure in operation and unwanted operation of distance relay with conventional mho or quadrilateral characteristic. Different from the fixed operation zones of conventional mho and quadrilateral characteristics, the adaptive mho characteristic presented herein can adaptively adjust its operation zone to solve the aforementioned issues. The basic principle of adaptive mho characteristic-based distance protection is described and the uniform expression of adaptive setting impedance is derived. Subsequently, taking the fault characteristics of PV power plant into consideration, the method of solving the phase angle of fault current is presented, which is the key to calculating adaptive setting impedance. The performances of the proposed protection scheme are evaluated by extensive digital simulations. The proposed protection scheme exhibits satisfactory robustness against the fault resistance and excellent adaptability to different grid codes. It can not only discriminate the internal and external faults occurring in the lines emanating from the PV power plant but also correctly identify the fault direction.**

***Index Terms*—Adaptive mho characteristic, distance protection, grid codes, photovoltaic (PV) power plant.**

I. Introduction

As a CLEAN way to generate electricity, grid-connected photovoltaic (PV) generation is a promising candidate to alleviate energy crisis and environmental problems, attracting the widespread attention of governments, researchers, and engineers [1]–[3]. As a result, many large-scale PV power plants have been put into operation or are under construction worldwide. Large-scale PV power plants are usually integrated into power grid via high-voltage transmission lines in which distance protection is widely applied [4]. However, significant differences between fault behaviors of synchronous sources and PV power plants may hinder the correct operation of conventional distance protection [5]. To solve this problem, this article aims to propose a new distance protection scheme for unbalanced faults that account for the majority of faults, applicable to transmission lines emanating from PV power plants.

Duo to the existence of fault resistance, distance relays are prone to underreach or overreach problems, causing distance relay's incorrect operation. To improve the immunity of distance relay against the fault resistance, new line fault impedance estimation algorithms [6]–[10], adaptive distance protection schemes [11], [12], and some other distance relaying schemes [13], [14] have been proposed to protect conventional transmission lines whose both ends are connected to synchronous sources. Compared with synchronous source, the amplitudes of positive- and negative-sequence fault currents of PV power plants are much smaller and their phase angles are significantly affected by grid codes that grid-connected inverters comply with. Therefore, there is a profound difference between fault behaviors of PV power plants and synchronous sources [15]. However, these proposed schemes did not consider the exclusive fault behaviors of PV power plants.

Distance protection schemes that are applicable to transmission lines emanating from doubly fed induction generator(DIG)-based wind farm have been well studied and presented in [16]–[19]. However, because of different topologies and control strategies, the fault behaviors of DFIG-based wind farms are quite different from those of PV power plants, especially when the crowbar of DFIG is activated [19], [20]. Jia *et al.* [21] studied the impact of voltage source converter (VSC) control strategies on distance protection and pointed that constant active power and balanced current control strategies favor the performances of distance protection. Hooshyar *et al.* [22] unveiled that distance relays of lines connected to full-scale converter-interfaced renewable energy power plants may miss trip for in-zone faults or incorrectly trip for out-of-zone faults. To solve this issue, Hooshyar *et al.* [23] presented a new scheme that requires a communication channel. Therefore, the reliability of the new scheme depends mainly on the communication channel. An improved distance protection scheme without the need for a communication channel was proposed to protect transmission line emanating from inverter-interfaced renewable energy generators (IIREGs) [24]. For distance relay on IIREG side, a long trigger delay is inevitable in the case of ungrounded short-circuit internal faults. Jia *et al*. [25] presented an active distance protection scheme based on harmonic current injection for PV dc-boosting integration system. Then, the adverse

Manuscript received February 24, 2020; revised June 17, 2020; accepted July 12, 2020. Date of publication August 24, 2020; date of current version August 26, 2021. This work was supported in part by the National Natural Science Foundation of China under Grant 51707193 and Grant 61703405, in part by the Fundamental Research Funds for the Central Universities under Grant 2020YQJD01, and in part by the Yue Qi Young Scholar Project of the China University of Mining and Technology (Beijing), Beijing, China. *(Corresponding author: Yingyu Liang.)*

The authors are with the School of Mechanical Electronic and Information Engineering, China University of Mining and Technology (Beijing), Beijing 100083, China (e-mail: liangyingyu2013@163.com; lmmx1995@163.com; wentingzha@126.com).

Digital Object Identifier 10.1109/JSYST.2020.3015225

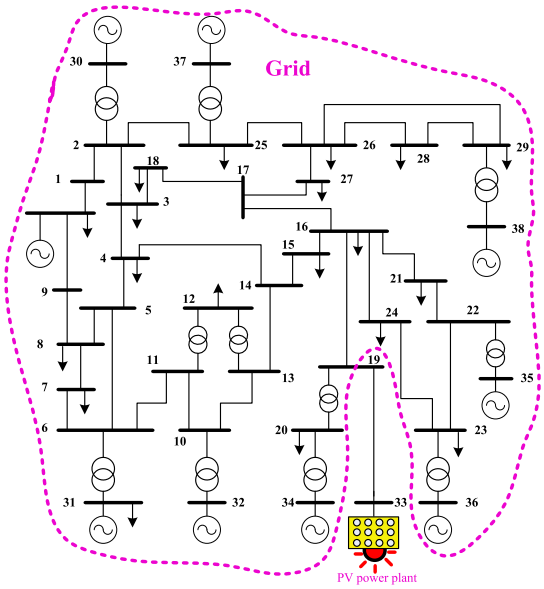

Fig. 1. Modified IEEE 39-bus New England system with a PV power plant.

effect of fault resistance can be mitigated by measuring the harmonic impedance. However, the injected harmonic current would degrade the power quality of output current, and a more complicated control strategy is required.

In this article, adaptive mho characteristic-based distance protection is presented to protect the lines emanating from the PV power plants. Frist, the correctness proof of adaptive mho characteristic is provided, which indicates that distance relay with adaptive mho characteristic can accurately discriminate internal and external faults. Then, according to the geometrical relationship of the measured impedance, additional impedance, setting impedance, and adaptive setting impedance, the uniform expression of adaptive setting impedance is derived. Subsequently, considering the exclusive fault behaviors of the PV power plant, the method of solving the phase angle of the fault current is proposed. Finally, the simulation results confirm the excellent performance of the proposed protection scheme under various conditions, including different fault locations, different fault resistances, different unbalanced fault types, and different grid codes.

II. System Description

For later analysis, a modified 230 kV, 60 Hz IEEE 39-bus New England system is established as shown in Fig. 1. Bus 33 is connected to a PV power plant (PVPP) with a capacity of 150 MW. The positive- and zero-sequence impedances of line 33–19 are 0.0617+j 0.325 and 0.227+j0.78 Ω/km, respectively. The positive- and zero-sequence capacitances of line 33–19 are 0.0086 and 0.0061 μF/km, respectively. The line length is 200 km. The parameters of main transformer are: S = 200 MVA, rated transformation ratio is 230/37 kV, $X_T = 0.16$ p.u., $R_T = 0.0355$ p.u. Other parameters of IEEE 39-bus system can be found in [26] and [27].

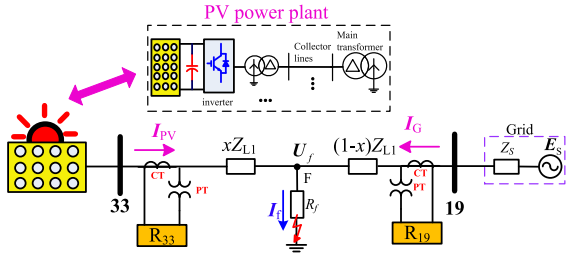

Fig. 2. Equivalent model of the modified IEEE 39-bus system with a PVPP.

Fig. 2 shows the equivalent model of the modified IEEE 39-bus system with a PVPP. In Fig. 2, $\boldsymbol{I}_{\rm PV}$ and $\boldsymbol{I}_{\rm G}$ are currents on PVPP side and grid side of line 33–19, respectively. $\boldsymbol{U}_f$ and $\boldsymbol{I}_f$ are the voltage at the fault point and current flowing through the fault path, respectively. R_f is fault resistance. x is the fault distance from bus 33 to fault point F as a percentage of the total length of line 33–19. $x > 0$ for forward faults and $x<0$ for reverse faults. Z_{L1} is the positive-sequence impedance of line 33–19. There are two distance relays, i.e., relays R_{33} and R_{19} that are on the PVPP side and grid side, respectively. Compared with relay R_{19}, PVPP has greater influence on relay R_{33} [24]. Therefore, relay R_{33} is taken as an example to present a solution to performance problems of distance protection of lines connected to PVPPs.

When a fault occurs at line 33–19, the measured impedance of relay R_{33} is expressed as

$$Z_m = \frac{\boldsymbol{U}_m}{\boldsymbol{I}_m} = xZ_{L1} + \Delta Z = xZ_{L1} + \frac{\boldsymbol{I}_f}{\boldsymbol{I}_m} R_f \qquad (1)$$

where $\boldsymbol{U}_m$ and $\boldsymbol{I}_m$ are measured voltage and current of relay R_{33}, respectively. ΔZ is the additional impedance caused by fault resistance R_f, causing an error between measured impedance of distance relay Z_m and the actual line fault impedance xZ_{L1}.

As stated in [24], owing to the unique fault behaviors of the grid-connected inverter, the additional impedance on the PVPP side is a large inductive or capacitive one, potentially causing distance relay failure in operation or unwanted operation. This article aims to propose an adaptive mho characteristic-based distance protection scheme to solve this problem.

III. Adaptive Mho Characteristic-Based Distance Protection

A. Basic Principle

The tripping characteristic for a mho relay can be expressed by an amplitude comparator with two inputs S_{1A} and S_{2A} as follows:

$$S_{1A} = Z_m - \frac{1}{2}Z_{\rm set} \quad \text{and} \quad S_{2A} = \frac{1}{2}Z_{\rm set} \qquad (2)$$

where $Z_{\rm set}$ is the setting impedance, which is set as $0.8Z_{L1}$ in this article, i.e., $Z_{\rm set} = 0.8Z_{L1}$. This indicates that the protected zone covers 80% of line 33–19.

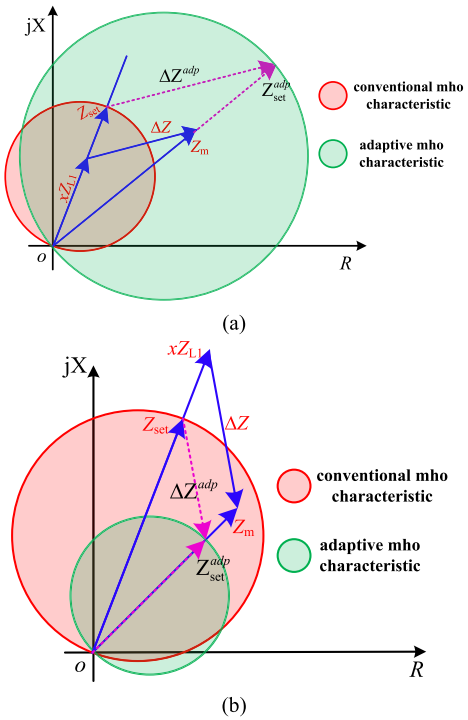

Fig. 3. Basic principle of adaptive mho characteristic. (a) Internal fault. (b) External fault.

Mathematically, internal and external faults can be distinguished by the following criterion:

$$\begin{cases} |S_{1A}| \le |S_{2A}|, & \text{internal fault} \\ |S_{1A}| > |S_{2A}|, & \text{external fault.} \end{cases} \tag{3}$$

When a bolted fault occurs, fault resistance is zero, causing $Z_m = xZ_{L1}$. If the fault is in the protected zone, i.e., $x < 0.8$, $|\mathrm{S}_{1A}|$must be less than $|\mathrm{S}_{2A}|$. If the fault is outside the protected zone, i.e., $x > 0.8$, $|\mathrm{S}_{1A}|$must be greater than $|\mathrm{S}_{2A}|$. Therefore, distance relay can correctly distinguish between internal and external faults when fault resistance is zero. However, in most cases, fault resistance is nonzero, introducing an error ΔZ between the measured impedance Z_m and the actual line fault impedance xZ_{L1}. As shown in Fig. 3(a), ΔZ may cause the underreach problem, and thereby distance relay loses dependability for internal faults. Also, ΔZ may cause the overreach problem, as shown in Fig. 3(b), and thereby distance relay loses security for external faults.

From (1), the additional impedance ΔZ is affected by the fault current, the measured current, and the fault resistance, which have to do with the control strategy, overcurrent capacity of PVPPs, and fault conditions. As a result, the measured impedance varies with ΔZ. However, no matter how the measured impedance varies, the operation zone of conventional mho characteristic remains unchanged. This results in a high risk of incorrect operations of the distance relay.

Based on the previous analysis, a fixed mho characteristic is not conducive to the correct operation of the distance relay. To solve the underreach and overreach problems, an adaptive mho characteristic-based distance protection is presented. Its basic principle is shown in Fig. 3. As shown in Fig. 3(a) and (b), the operation zone of adaptive mho characteristic is adaptively enlarged to overcome the underreach problem and reduced to overcome the overreach problem. Then, the adverse effect caused by fault resistance is eliminated, and distance relay with adaptive mho characteristic can operate correctly, which will be further confirmed mathematically in the following section.

1) Correctness Proof of Adaptive Mho Characteristic: From Fig. 3, adaptive setting impedance is expressed as

$$Z_{\mathrm{set}}^{\mathrm{adp}} = Z_{\mathrm{set}} + \Delta Z^{\mathrm{adp}}. \tag{4}$$

Moreover, the following relations can also be obtained:

$$\begin{cases} \arg\left(Z_{L1}\right) = \arg\left(Z_{\mathrm{set}}\right) \\ \arg\left(Z_m\right) = \arg\left(Z_{\mathrm{set}}^{\mathrm{adp}}\right) \\ \arg\left(\Delta Z\right) = \arg\left(\Delta Z^{\mathrm{adp}}\right). \end{cases} \tag{5}$$

According to the geometrical relationship of impedances shown in Fig. 3, ΔZ^{adp} can be expressed as follows:

$$\Delta Z^{\mathrm{adp}} = \frac{Z_{\mathrm{set}}}{xZ_{L1}} \cdot \Delta Z. \tag{6}$$

For adaptive mho characteristic, two inputs S_{1A} and S_{2A} of the amplitude comparator can be expressed as follows:

$$S_{1A} = Z_m - \frac{1}{2}Z_{\mathrm{set}}^{\mathrm{adp}} \text{and} S_{2A} = \frac{1}{2}Z_{\mathrm{set}}^{\mathrm{adp}}. \tag{7}$$

Based on (1), (4), (6), and (7), we can obtain

$$\begin{aligned} |S_{1A}| &= \left| Z_m - \frac{1}{2}Z_{\mathrm{set}}^{\mathrm{adp}} \right| \\ &= \left| xZ_{L1} + \Delta Z - \frac{1}{2}\left(Z_{\mathrm{set}} + \frac{Z_{\mathrm{set}}}{xZ_{L1}} \cdot \Delta Z \right) \right| \\ &= \left| 1 + \frac{\Delta Z}{xZ_{L1}} \right| \left| xZ_{L1} - \frac{1}{2}Z_{\mathrm{set}} \right| \end{aligned} \tag{8}$$

$$\begin{aligned} |S_{2A}| &= \left| \frac{1}{2}Z_{\mathrm{set}}^{\mathrm{adp}} \right| = \frac{1}{2}\left| Z_{\mathrm{set}} + \frac{Z_{\mathrm{set}}}{xZ_{L1}} \cdot \Delta Z \right| \\ &= \left| 1 + \frac{\Delta Z}{xZ_{L1}} \right| \left| \frac{1}{2}Z_{\mathrm{set}} \right|. \end{aligned} \tag{9}$$

Thus, the ratio of $|\mathrm{S}_{1A}|$ over $|\mathrm{S}_{2A}|$ is derived as

$$\frac{|S_{1A}|}{|S_{2A}|} = \frac{\left| xZ_{L1} - \frac{1}{2}Z_{\mathrm{set}} \right|}{\left| \frac{1}{2}Z_{\mathrm{set}} \right|} = \frac{|xZ_{L1} - 0.4Z_{L1}|}{|0.4Z_{L1}|} = \frac{|x - 0.4|}{0.4}. \tag{10}$$

As seen from (10), the ratio of $|\mathrm{S}_{1A}|$ over $|\mathrm{S}_{2A}|$ is unaffected by ΔZ, and thereby the adverse effect of the fault resistance is eliminated.

For internal faults, $x \le 0.8$, $|\mathrm{S}_{1A}|$ is less than or equal to $|\mathrm{S}_{2A}|$. For external faults, $x > 0.8$, $|\mathrm{S}_{1A}|$ is greater than $|\mathrm{S}_{2A}|$. Therefore, when adaptive mho characteristic is applied in distance relay, the criterion (3) can be utilized to correctly discriminate between internal and external faults.

It should be noted that only forward faults were discussed. When reverse faults occur, the fault distance x is less than zero,

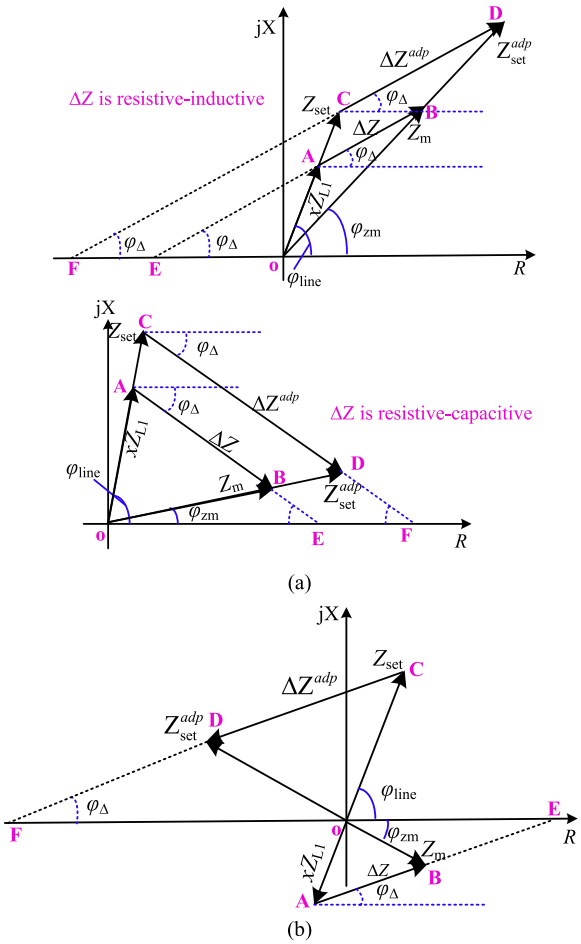

Fig. 4. Impedance complex plane. (a) Forward fault. (b) Reverse fault.

i.e., $x < 0$. According to (10), $|S_{1A}|$ is greater than $|S_{2A}|$. Therefore, the reverse faults are correctly identified as the external faults.

2) Calculation of Adaptive Setting Impedance: Adaptive setting impedance $Z_{\text{set}}^{\text{adp}}$ is the key of adaptive mho characteristic. To correctly identify the internal and external faults, adaptive setting impedance must first be calculated.

The geometrical relationship of impedances is shown in Fig. 4. In Fig. 4, φ_Δ, φ_{zm}, and φ_{line} are phase angles of the additional impedance, measured impedance, and line impedance, respectively.

For forward faults, the geometrical relationship of impedances is shown in Fig. 4(a). If ΔZ is resistive–inductive, $\varphi_\Delta > 0$. If ΔZ is resistive–capacitive, $\varphi_\Delta < 0$. From Fig. 4(a), the following relations can be obtained:

$$\begin{cases} \varphi_\Delta > 0 \\ \angle\text{FCO} = \varphi_{\text{line}} - \varphi_\Delta \\ \angle\text{FDO} = \varphi_{zm} - \varphi_\Delta \\ \angle\text{DFO} = \angle\text{CFO} = \varphi_\Delta \end{cases} \quad \begin{cases} \varphi_\Delta < 0 \\ \angle\text{FCO} = \pi + \varphi_\Delta - \varphi_{\text{line}} \\ \angle\text{FDO} = \pi - \varphi_{zm} + \varphi_\Delta \\ \angle DFO = \angle\text{CFO} = -\varphi_\Delta \end{cases} \tag{11}$$

$$\text{OC} = |Z_{\text{set}}|, \quad \text{OD} = \left|Z_{\text{set}}^{\text{adp}}\right|. \tag{12}$$

Applying the law of sines to ΔCFO, the following relation is established:

$$\frac{\text{OF}}{\sin\angle\text{FCO}} = \frac{\text{OC}}{\sin\angle\text{CFO}}. \tag{13}$$

According to (11)–(13), OF is expressed as

$$\text{OF} = \text{sgn}(\varphi_\Delta)\frac{\sin(\varphi_{\text{line}} - \varphi_\Delta)}{\sin\varphi_\Delta}|Z_{\text{set}}| \tag{14}$$

where sgn() represents the sign function.

Applying the law of sines to ΔDFO, the following relation is established:

$$\frac{\text{OF}}{\sin\angle\text{FDO}} = \frac{\text{OD}}{\sin\angle\text{DFO}}. \tag{15}$$

According to (11), (12), and (15), OD is expressed as

$$\text{OD} = \left|Z_{\text{set}}^{\text{adp}}\right| = \text{sgn}(\varphi_\Delta)\cdot\text{OF}\cdot\frac{\sin\varphi_\Delta}{\sin(\varphi_{zm} - \varphi_\Delta)}. \tag{16}$$

Combining (14) and (16), we can obtain

$$\left|Z_{\text{set}}^{\text{adp}}\right| = \frac{\sin(\varphi_{\text{line}} - \varphi_\Delta)}{\sin(\varphi_{zm} - \varphi_\Delta)}|Z_{\text{set}}|. \tag{17}$$

As shown in Fig. 4(a), in the case of forward faults, $Z_{\text{set}}^{\text{adp}}$ and Z_m have the same phase angle. Thus

$$Z_{\text{set}}^{\text{adp}} = \frac{\sin(\varphi_{\text{line}} - \varphi_\Delta)}{\sin(\varphi_{zm} - \varphi_\Delta)}|Z_{\text{set}}|\angle\varphi_{zm}. \tag{18}$$

For reverse faults, the geometrical relationship of impedances is shown in Fig. 4(b). Due to space constraints, the case that ΔZ is resistive–capacitive is not presented.

From Fig. 4(b), the following relations can be obtained:

$$\begin{aligned} &\angle\text{FCO} = \varphi_{\text{line}} - \varphi_\Delta, \angle\text{FDO} = \pi + \varphi_{zm} - \varphi_\Delta \\ &\angle\text{DFO} = \angle\text{CFO} = \varphi_\Delta, \text{OC} = |Z_{\text{set}}|, \text{OD} = \left|Z_{\text{set}}^{\text{adp}}\right|. \end{aligned} \tag{19}$$

Based on (19) and applying the law of sines to ΔCFO and ΔDFO, $|Z_{\text{set}}^{\text{adp}}|$ is derived as follows:

$$\left|Z_{\text{set}}^{\text{adp}}\right| = \frac{\sin(\varphi_{\text{line}} - \varphi_\Delta)}{\sin(\varphi_\Delta - \varphi_{zm})}|Z_{\text{set}}|. \tag{20}$$

As shown in Fig. 4(b), in the case of reverse faults, phase angles of $Z_{\text{set}}^{\text{adp}}$ and Z_m satisfy the following relation:

$$\arg\left(Z_{\text{set}}^{\text{adp}}\right) = \arg(Z_{\text{m}}) + \pi = \varphi_{zm} + \pi. \tag{21}$$

Thus

$$\begin{aligned} Z_{\text{set}}^{\text{adp}} &= \frac{\sin(\varphi_{\text{line}} - \varphi_\Delta)}{\sin(\varphi_\Delta - \varphi_{zm})}|Z_{\text{set}}|\angle(\varphi_{\text{zm}} + \pi) \\ &= \frac{\sin(\varphi_{\text{line}} - \varphi_\Delta)}{\sin(\varphi_{zm} - \varphi_\Delta)}|Z_{\text{set}}|\angle\varphi_{\text{zm}}. \end{aligned} \tag{22}$$

Comparing (18) and (22), they have the same expression. Therefore, regardless of the forward or reverse fault, adaptive setting impedance can be uniformly expressed as

$$Z_{\text{set}}^{\text{adp}} = K_a|Z_{\text{set}}|\angle\varphi_{\text{zm}} \tag{23}$$

where K_a is the adaptive coefficient, which is expressed as

$$K_a = \frac{\sin\left(\varphi_{\text{line}} - \varphi_\Delta\right)}{\sin\left(\varphi_{zm} - \varphi_\Delta\right)}. \tag{24}$$

Based on (17), (20), and (24), $K_a > 0$ in the case of the forward faults; $K_a < 0$ in the case of the reverse faults. Thus, K_a can be utilized to identify the fault direction.

After adaptive setting impedance is calculated, the internal and external faults can be correctly identified by the distance relay with adaptive mho characteristic. Considering the reliability of distance relay, the protection criterion is developed as follows:

Internal fault: A fault occurs and $|Z_m - \frac{1}{2}Z_{\text{set}}^{\text{adp}}| \le |\frac{1}{2}Z_{\text{set}}^{\text{adp}}|$ for a continuous 6 ms.

External fault: A fault occurs and it is not identified as an internal fault.

In (23) and (24), Z_{set} and φ_{line} are known. φ_{zm} can be can be obtained by Fourier algorithm. According to (1), φ_Δ can be expressed as

$$\varphi_\Delta = \arg\left(\boldsymbol{I}_f\right) - \arg\left(\boldsymbol{I}_m\right). \tag{25}$$

$\boldsymbol{I}_m$ can be measured, and thereby $\arg(\boldsymbol{I}_m)$ can be obtained by discrete Fourier algorithm. However, fault current $\boldsymbol{I}_f$is immeasurable. This indicates that $\arg(\boldsymbol{I}_f)$cannot be obtained directly. However, $\arg(\boldsymbol{I}_f)$is the basis and prerequisite for calculating adaptive setting impedance. Therefore, the method of solving $\arg(\boldsymbol{I}_f)$is particularly important, which will be explained in detail in the following subsection.

B. *Method of Solving* $\arg(\boldsymbol{I}_f)$

For power grids with synchronous sources, the method of solving $\arg(\boldsymbol{I}_f)$ has been presented in [9]. However, PVPPs exhibit exclusive fault behaviors that significantly differ from those of synchronous sources. This leads to the failure of the conventional method designed for power grids with synchronous sources. Taking exclusive fault behaviors of the PVPP into consideration, the method of solving $\arg(\boldsymbol{I}_f)$ is presented under unbalanced faults.

1) Single-Phase-to-Ground Fault: Considering an AG fault as an example, the fault current $\boldsymbol{I}_f$ is expressed as follows:

$$\boldsymbol{I}_f = \boldsymbol{I}_{fa} = \boldsymbol{I}_{fa1} + \boldsymbol{I}_{fa2} + \boldsymbol{I}_{fa0} = 3\boldsymbol{I}_{fa0}. \tag{26}$$

$\arg(\boldsymbol{I}_f)$ can be obtained as follows:

$$\arg\left(\boldsymbol{I}_f\right) = \arg\left(\boldsymbol{I}_{f0}\right) = \arg\left(\frac{\boldsymbol{I}_{\text{PV0}}}{\boldsymbol{C}_0}\right) \tag{27}$$

where $\boldsymbol{C}_0$ is zero-sequence current distribution factor. Since zero-sequence current is unaffected by the PVPP, $\boldsymbol{C}_0$ is almost a real number, i.e., $\arg(\boldsymbol{C}_0) \approx 0°$. Thus, (27) can be simplified to

$$\arg\left(\boldsymbol{I}_f\right) \approx \arg\left(\boldsymbol{I}_{\text{PV0}}\right). \tag{28}$$

2) Phase-to-Phase Fault: Considering a BC fault as an example, the fault current $\boldsymbol{I}_f$ is expressed as follows:

$$\boldsymbol{I}_f = \boldsymbol{I}_{fb} - \boldsymbol{I}_{fc} = \left(a^2 - a\right)\left(\boldsymbol{I}_{fa1} - \boldsymbol{I}_{fa2}\right) \tag{29}$$

where $a = e^{\text{j}2\pi/3}$.

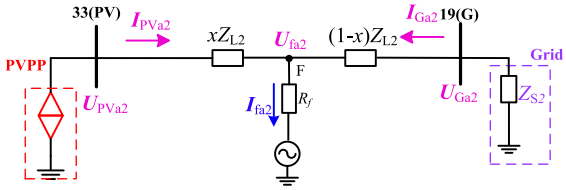

Fig. 5. Phase A negative-sequence network of the circuit shown in Fig. 2.

For a BC fault, the relation that $\boldsymbol{I}_{fa1} = -\boldsymbol{I}_{fa2}$ is satisfied, so

$$\boldsymbol{I}_f = -2\left(a^2 - a\right)\boldsymbol{I}_{fa2} = \text{j}2\sqrt{3}\boldsymbol{I}_{fa2}. \tag{30}$$

Phase A negative-sequence network of the circuit shown in Fig. 2 is displayed in Fig. 5. In Fig. 5, the subscript "2" represents negative-sequence components. To ensure balanced output current and avoid overcurrent of power electronic components, negative-sequence current of grid-connected inverter in the PVPP is generally eliminated in the case of unbalanced short-circuit faults. It indicates that $\boldsymbol{I}_{\text{PV}a2}$ is approximately equal to zero, and thereby the following relations can be obtained:

$$\boldsymbol{I}_{fa2} \approx \boldsymbol{I}_{Ga2}, \quad \boldsymbol{U}_{\text{PV}a2} \approx \boldsymbol{U}_{fa2}. \tag{31}$$

Thus

$$\boldsymbol{I}_{fa2} \approx -\frac{\boldsymbol{U}_{\text{PV}a2}}{(1-x)\,Z_{L2} + Z_{S2}}. \tag{32}$$

Generally, negative impedances of the grid and line have a similar phase angle, i.e.,

$$\arg\left(Z_{S2}\right) \approx \arg\left(Z_{L2}\right) = \varphi_{\text{line}}. \tag{33}$$

From (32) and (33), we can obtain

$$\arg\left(\boldsymbol{I}_{fa2}\right) \approx \arg\left(\boldsymbol{U}_{\text{PV}a2}\right) - \varphi_{\text{line}} - \pi. \tag{34}$$

According to (30) and (34), $\arg(\boldsymbol{I}_f)$ is expressed as

$$\arg\left(\boldsymbol{I}_f\right) \approx \arg\left(\boldsymbol{U}_{\text{PV}a2}\right) - \varphi_{\text{line}} - \frac{\pi}{2}. \tag{35}$$

Because the voltage at bus 33 can be measured, $\arg(\boldsymbol{U}_{\text{PV}a2})$ can be obtained by discrete Fourier algorithm. As a result, $\arg(\boldsymbol{I}_f)$ is obtained.

3) Phase-to-Phase-to-Ground Fault: Considering a BCG fault as an example, the fault current $\boldsymbol{I}_f$ is expressed as follows:

$$\begin{aligned}\boldsymbol{I}_f &= \boldsymbol{I}_{f\text{b}} - \boldsymbol{I}_{f\text{c}} = -\text{j}\sqrt{3}\left(\boldsymbol{I}_{fa1} - \boldsymbol{I}_{fa2}\right) \\ &= -\text{j}\sqrt{3}\left(\frac{\Delta\boldsymbol{I}_{\text{PV}a1}}{\boldsymbol{C}_1} - \frac{\boldsymbol{I}_{\text{PV}a2}}{\boldsymbol{C}_2}\right).\end{aligned} \tag{36}$$

For conventional power grid without PVPPs, $\boldsymbol{C}_1 = \boldsymbol{C}_2$ and $\arg(\boldsymbol{C}_1) \approx 0°$ in (36), so

$$\arg\left(\boldsymbol{I}_f\right) \approx \arg\left(\Delta\boldsymbol{I}_{\text{PV}a1} - \boldsymbol{I}_{\text{PV}a2}\right) - \frac{\pi}{2}. \tag{37}$$

However, the integration of PVPPs leads to the untenable conditions of $\boldsymbol{C}_1 = \boldsymbol{C}_2$ and $\arg(\boldsymbol{C}_1) \approx 0°$. Consequently, $\arg(\boldsymbol{I}_f)$ cannot be obtained by (37). To tackle this issue, a new formula of measured impedance is developed.

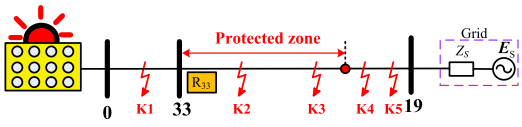

Fig. 6. Schematic diagram of different fault locations.

When a BCG occurs, the measured voltages of phase B and phase C at the relay point are expressed as

$$\boldsymbol{U}_{\mathrm{PV}b} = (\boldsymbol{I}_{PVb} + 3K\boldsymbol{I}_{\mathrm{PV0}}) \cdot xZ_{L1} + \boldsymbol{I}_{fb}R_f \tag{38}$$

$$\boldsymbol{U}_{\mathrm{PV}c} = (\boldsymbol{I}_{\mathrm{PV}c} + 3K\boldsymbol{I}_{\mathrm{PV0}}) \cdot xZ_{L1} + \boldsymbol{I}_{fc}R_f. \tag{39}$$

The summation of (38) and (39) results in a new formula of measured impedance in the case of a BCG fault [23]

$$\begin{aligned} Z_m &= \frac{\overbrace{\boldsymbol{U}_{\mathrm{PV}b} + \boldsymbol{U}_{\mathrm{PV}c}}^{\boldsymbol{U}_{\mathrm{m}}}}{\underbrace{\boldsymbol{I}_{\mathrm{PV}b} + \boldsymbol{I}_{\mathrm{PV}c} + 6K\boldsymbol{I}_{\mathrm{PV0}}}_{\boldsymbol{I}_m}} \\ &= xZ_{L1} + \underbrace{\frac{\overbrace{\boldsymbol{I}_{fb} + \boldsymbol{I}_{fc}}^{\boldsymbol{I}_f}}{\underbrace{\boldsymbol{I}_{\mathrm{PV}b} + \boldsymbol{I}_{\mathrm{PV}c} + 6K\boldsymbol{I}_{\mathrm{PV0}}}_{\boldsymbol{I}_m}} R_f}_{\Delta Z} \end{aligned} \tag{40}$$

where K is zero-sequence compensation factor and $K = (Z_{L0} - Z_{L1})/(3Z_{L1})$. Thus

$$\arg(\boldsymbol{I}_f) = \arg(\boldsymbol{I}_{fb} + \boldsymbol{I}_{fc}) = \arg\left(\frac{\boldsymbol{I}_{\mathrm{PV0}}}{\boldsymbol{C}_0}\right) \approx \arg(\boldsymbol{I}_{\mathrm{PV}=0}). \tag{41}$$

IV. Performance Evaluation

The modified IEEE 39-bus New England system is established in PSCAD/EMTDC. A series of simulations under various conditions are conducted to evaluate the performances of the proposed protection scheme.

A. Performance Evaluation Under Different Fault Locations

To evaluate the performance of the proposed protection scheme under different fault locations including forward and reverse directions, a 50-km line 0–33 is connected between the PVPP and bus 33 as shown in Fig. 6. The parameters of line 0–33 are same as those of line 33–19. The five fault locations K1–K5 are shown in Fig. 6, which are set at 20%, 30%, 70%, 90%, 97% from bus 33. The faults at K2 and K3 are inside the protected zone of relay R_{33}, and thereby they are the internal faults. The faults at K1, K4, and K5 are outside the protected zone of relay R_{33}, and thereby they are the external faults.

The distance protection with mho or quadrilateral characteristic is widely applied in practical engineering, called the implemented scheme herein. The measured impedance Z_m at relay point is the ratio of the measured voltage $\boldsymbol{U}_m$ over the measured current $\boldsymbol{I}_m$, as shown in (1). When a fault occurs, if the measured impedance Z_m enters into the operation zone of mho or quadrilateral characteristic, this fault is identified as an internal fault. Otherwise, this fault is identified as an external fault. This is the basic principle of the implemented scheme. The performance of the implemented scheme will be compared with that of the proposed scheme under different fault locations.

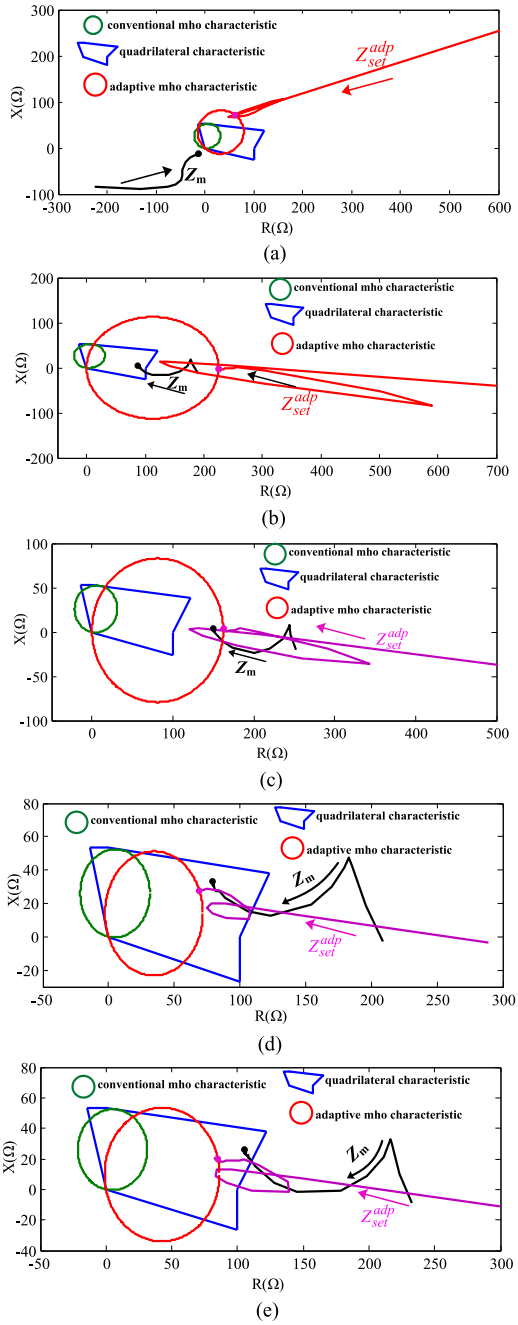

Fig. 7. Simulation results under different fault locations. (a) K1. (b) K2. (c) K3. (d) K4. (e) K5.

Assume that phase A-to-ground faults occur at K1−K5 and the PVPP complies with Chinese grid code (Chinese GC) [28]. Fig. 7(a)–(e) show the simulation results under different fault locations K1−K5. In Fig. 7(a), the measured impedance Z_m is outside all the operation zones in steady state so that

TABLE I
FAULT IDENTIFICATION RESULTS UNDER DIFFERENT FAULT LOCATIONS

Fault location	Fault resistance (Ω)	Conventional mho characteristic		Quadrilateral characteristic		Adaptive mho characteristic	
K1	10	E	√	E	√	E	√
K2	50	E	×	I	√	I	√
K3	50	E	×	E	×	I	√
K4	10	E	√	I	×	E	√
K5	10	E	√	I	×	E	√

the fault at K1 is identified as an internal fault by distance relays with conventional mho, quadrilateral, and adaptive mho characteristics. From Fig. 7(b), the measured impedance Z_m enters into the operation zones of quadrilateral and adaptive mho characteristics in steady state; however, it is outside the operation zone of conventional mho characteristic. Consequently, the fault occurring at K2 is identified as an external fault by distance relay with conventional mho characteristic and an internal fault by distance relays with quadrilateral and adaptive mho characteristics. The same analysis process is applied to Fig. 7(c)–(e). Based on the analysis of Fig. 7(a)–(e), the fault identification results under different fault locations are summarized in Table I.

In Table I, "I" and "E" indicate that the fault is identified as internal and external faults, respectively. "√" and "×" denote that the fault identification result is correct and incorrect, respectively. As seen from Table I, distance relays with conventional mho and quadrilateral characteristics have a high probability of misidentifying the internal and external faults, resulting in failure in operation or undesirable operation of distance relay. By contrast, distance relay with adaptive mho characteristic can accurately identify the internal and external faults, irrespective of the fault location.

The adaptive coefficients (K_a) corresponding to fault locations K1–K5 are 1.78, 4.26, 3.07, 1.41, and 1.65 in steady state. K_a of the fault at K1 is negative, while K_a of the faults at K2–K5 are all positive. As a result, the fault point K1 is identified in the reverse direction of the protected zone, while the fault points K2–K5 are identified in the forward direction of the protected zone.

From the above, the adaptive mho characteristic-based distance protection scheme can accurately identify the internal and external faults as well as the fault direction.

B. Performance Evaluation Under Different Fault Resistances

Table II shows the simulation results of the proposed protection scheme under phase-A-to-ground faults with different fault resistances, i.e., 1, 5, 25, 50, and 100 Ω. The fault locations are set at K3 and K4. From Table II, although the fault resistance varies over a wide range, the faults occurring at K3 are always correctly identified as the internal faults, while the faults occurring at K4 are always correctly identified as the external faults. The proposed protection scheme exhibits superior robustness against the fault resistance. Since the vast majority of faults occur with a fault resistance, excellent robustness against the fault resistance is very important for distance relay.

TABLE II
SIMULATION RESULTS UNDER DIFFERENT FAULT RESISTANCES

Fault resistance (Ω)	Fault location	Z_m(Ω)	Z_{set}^{adp} (Ω)	Result
1	K3	12.8+j44.2	14.6+j50.1	I
	K4	19.2+j55.5	16.8+j48.6	E
5	K3	28.8+j38.2	32.5+j43.1	I
	K4	48.1+j42.9	41.8+j37.3	E
25	K3	91.5+j17.8	101.0+j19.6	I
	K4	146.3+j9.5	124.5+j8.1	E
50	K3	148.2+j4.7	160.9+j5.1	I
	K4	219.2−j6.2	183.8−j5.2	E
100	K3	221.6−j9.5	235.2−j10.1	I
	K4	291.6−j23.8	240.7−j19.6	E

Cases shown in Fig. 8.

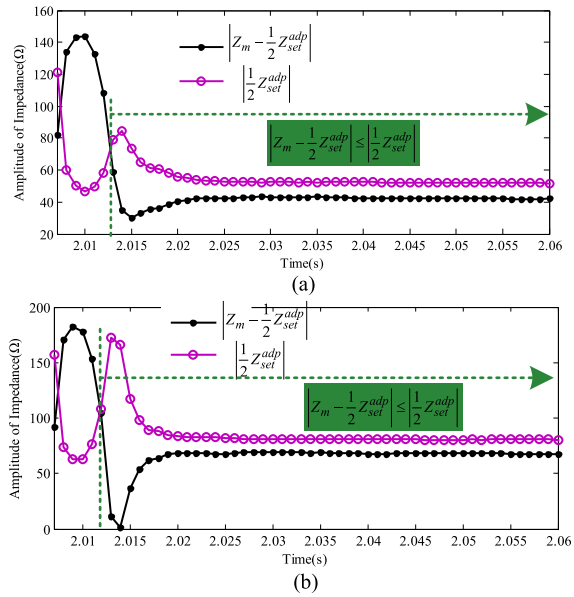

Fig. 8. Simulation waveforms of the chosen sample cases from Table II. (a) 25 Ω; K3. (b) 50 Ω; K3.

The simulation waveforms of chosen sample cases from Table II are displayed in Fig. 8(a) and (b). All the faults occur at $t = 2$ s. As shown in Fig. 8(a), $|Z_m - \frac{1}{2}Z_{\text{set}}^{\text{adp}}|$ is less than $|\frac{1}{2}Z_{\text{set}}^{\text{adp}}|$ at about 13 ms after fault inception. According to the protection criterion, the fault with a fault resistance of 25 Ω at K3 can be identified as the internal fault within 20 ms. As shown in Fig. 8(b), $|Z_m - \frac{1}{2}Z_{\text{set}}^{\text{adp}}|$ is less than $|\frac{1}{2}Z_{\text{set}}^{\text{adp}}|$ at about 12 ms after fault inception. According to the protection criterion, the fault with a fault resistance of 50 Ω at K3 can be also identified as the internal fault within 20 ms.

C. Performance Evaluation Under Different Types of Unbalanced Faults and Different Grid Codes

Table III shows the measured impedances and adaptive setting impedances in steady state under different types of unbalanced

TABLE III
SIMULATION RESULTS UNDER DIFFERENT TYPES OF UNBALANCED FAULTS AND DIFFERENT GRID CODES

Fault type	Fault location	Chinese GC			German GC			NA-GC		
		$Z_m(\Omega)$	$Z_{set}^{adp}(\Omega)$	Result	$Z_m(\Omega)$	$Z_{set}^{adp}(\Omega)$	Result	$Z_m(\Omega)$	$Z_{set}^{adp}(\Omega)$	Result
AG	K2	10.1+j17.7	26.8+j47.0	I	9.9+j18.0	26.1+j48.9	I	10.0+j17.8	26.6+j47.2	I
	K5	45.2+j47.5	36.4+j38.3	E	43.8+j50.2	35.3+j40.5	E	44.3+j49.3	35.7+j39.7	E
BC	K2	7.9+j0.88	20.8+j2.31	I	13.5+j2.11	35.6+j5.57	I	4.2+j1.03	11.0+j2.69	I
	K5	33.8−j13.7	26.9−j10.9	E	53.4−j6.26	42.8−j5.02	E	22.6−j15.9	17.4−j12.2	E
BCG	K2	7.0+j19.3	18.6+j51.3	I	6.9+19.5	18.2+j51.8	I	7.2+j19.2	19.2+j50.9	I
	K5	30.7+j60.3	24.8+j48.8	E	29.6+j61.8	23.9+j50.0	E	32.1+j59.1	25.9+j47.7	E

Cases shown in Fig. 9.

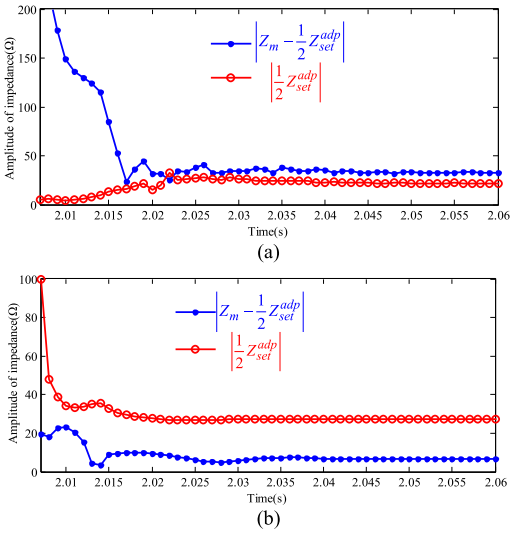

Fig. 9. Simulation waveforms of the chosen sample cases from Table III. (a) BC, K5, German GC. (b) BCG, K2, NA-GC.

faults and different grid codes. In this subsection, Chinese GC, German GC, and North American GC (NA-GC) are applied [22], [29]. As seen from Table III, in spite of the different fault types and grid codes, the proposed protection scheme can accurately identify the faults occurring at K2 and K5 as the internal and external faults, respectively. This indicates that the proposed scheme exhibits a good adaptability to different grid codes and different types of unbalanced faults.

The simulation waveforms of chosen sample cases from Table III are displayed in Fig. 9(a) and (b). All the faults occur at $t = 2$ s. From Fig. 9(a), $|Z_m - \frac{1}{2}Z_{\text{set}}^{\text{adp}}|$ is greater than $|\frac{1}{2}Z_{\text{set}}^{\text{adp}}|$, and thereby the fault occurring at K5 is correctly identified as the external fault under a BC fault and German GC. As shown in Fig. 9(b), $|Z_m - \frac{1}{2}Z_{\text{set}}^{\text{adp}}|$ is always less than $|\frac{1}{2}Z_{\text{set}}^{\text{adp}}|$ under a BCG fault and NA-GC. As a result, this fault occurring at K2 is correctly identified as the internal fault.

D. Comparison of the Proposed Scheme With Prior-Art Schemes

This subsection compares the proposed scheme with some prior-art schemes in the following five aspects:

TABLE IV
COMPARISON OF THE PROPOSED SCHEME WITH PRIOR-ART SCHEMES

Description	Implemented scheme	Scheme in [20]	Scheme in [23]	Scheme in [24]	Scheme in [25]	Proposed scheme
Robustness against fault resistance	Poor	Excellent	Average	Average	Good	Excellent
Whether the scheme can identify and indicate the fault direction	No	No	Yes	No	No	Yes
Whether a communication channel is required	No	Yes	Yes	No*	No	No
Whether the software of converter needs to be upgraded	No	No	No	No	Yes	No
Adaptability to different grid codes	Poor	Excellent	Average	Average	Excellent	Excellent

*However, distance relay may respond to the internal fault with a delay of 300 ms.

1) robustness against fault resistance;
2) whether the scheme can identify and indicate the fault direction;
3) whether a communication channel is required;
4) whether the software of converter needs to be upgraded;
5) adaptability to different grid codes.

The detailed comparison results of the proposed scheme and five prior-art schemes are shown in Table IV.

Compared with the implemented scheme, schemes in [23] and [24], the proposed scheme offers superior robustness against fault resistance and adaptability to different grid codes. Compared with the implemented scheme, schemes in [20] and [24], and [25], the proposed scheme has the ability to identify and indicate the fault direction. Compared with the proposed scheme, schemes in [20] and [23] require a communication channel, which increases hardware cost. Although the scheme in [24] does not require a communication channel, it does so at the cost of a very slow response speed for distance relay on the PVPP side.

The scheme in [25] proposes to inject fourth harmonic current into power grid. The fourth harmonic impedance is measured to distinguish between internal and external faults. In [25], it has been confirmed that the scheme based on harmonic current injection provides a good robustness against fault resistance in

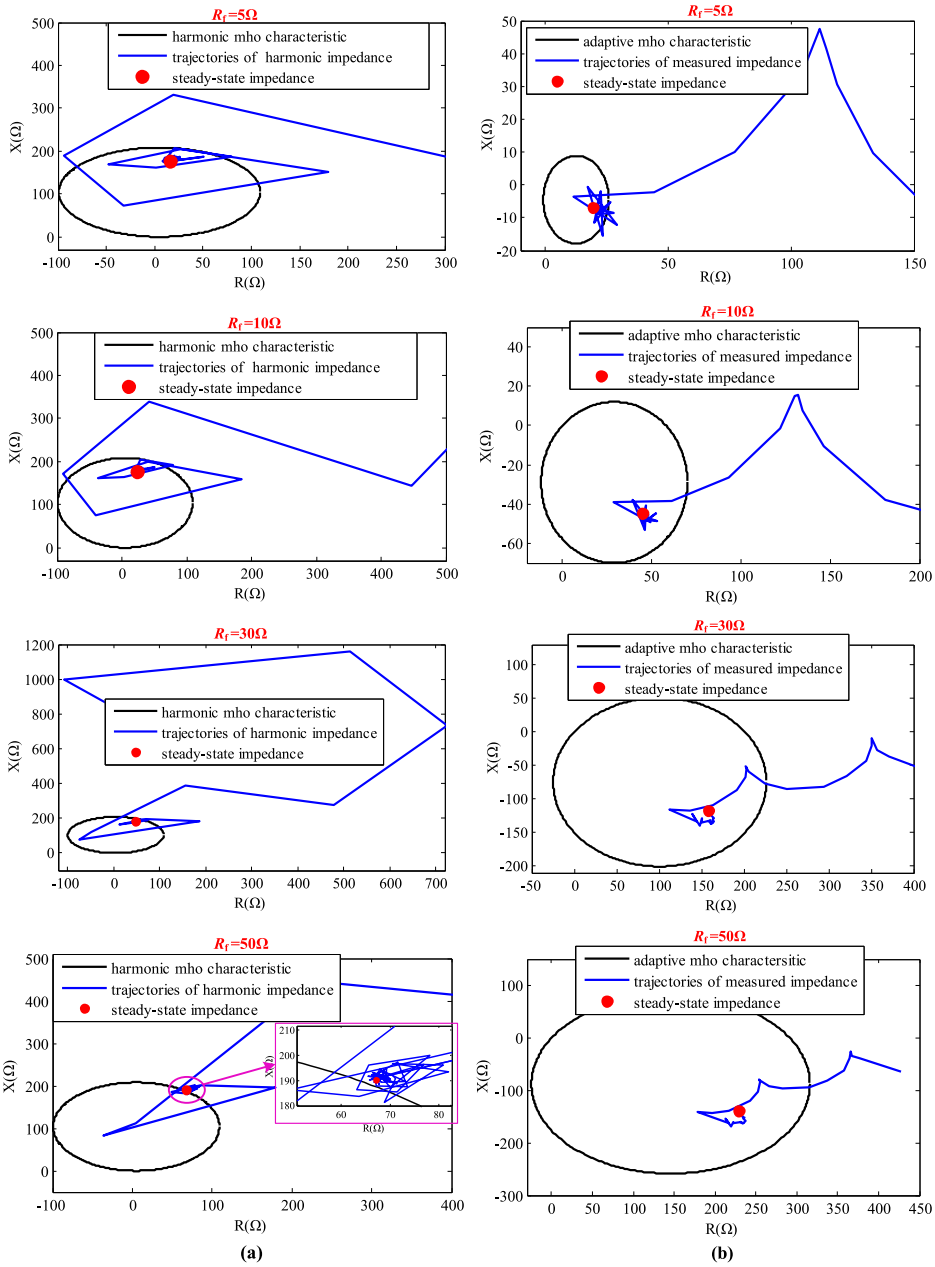

Fig. 10. Performance comparison of the scheme in [25] and the proposed scheme under different fault resistances. (a) Simulation results of the scheme in [25]. (b) Simulation results of the proposed scheme.

most cases. However, when the value of fault resistance is large, the scheme in [25] has the risk of misidentifying the internal faults, which will be verified below. In contrast, the proposed scheme offers better robustness against fault resistance. The scheme in [25] measures harmonic impedance that has nothing to do with the power–frequency components, and thereby this scheme remains unaffected by grid codes. In order to control the harmonic current, the software of the converter needs to be upgraded, which hinders the promotion and application of the scheme in [25].

According to the comparison results shown in Table IV and the foregoing analysis, the proposed scheme performs much better than prior-art schemes.

Considering the scheme in [25] as an example, its robustness against fault resistance is compared with that of the proposed scheme. Assuming that phase B-to-phase C faults occur with different fault resistances, the simulation results of the scheme in [25] and the proposed scheme are displayed in Fig. 10(a) and (b), respectively. The fault location of all faults is set at 60% of line 33–19 from bus 33, which is inside the protected zone of relay R_{33}. Therefore, all the faults are internal faults.

From Fig. 10(a), when fault resistance $R_f = 5$, 10, and 30 Ω, the harmonic impedances measured by distance relay enter into the operation zone of harmonic mho characteristic in steady state, so the faults with fault resistances of 5, 10, and 30 Ω are correctly identified as the internal faults. This indicates that

the scheme in [25] has a certain tolerance against fault resistance. However, when the value of fault resistance is large, e.g., $R_f = 50\,\Omega$, the harmonic impedance measured by distance relay is outside the operation zone of harmonic mho characteristic in steady state, as shown in Fig. 10(a). As a result, the fault with a fault resistance of $50\,\Omega$ is misidentified as an external fault, causing distance relay to fail to operate. In summary, the scheme in [25] performs well unless fault resistance is high. Therefore, its robustness against fault resistance is rated as "good" in Table IV.

From Fig. 10(b), irrespective of fault resistance, the impedances measured by distance relay always enter into the operation zone of adaptive mho characteristic in steady state. These faults with different fault resistances are correctly identified as the internal faults. The proposed scheme shows a better tolerance against fault resistance than the scheme in [25]. Therefore, its robustness against fault resistance is rated as "excellent" in Table IV.

V. Discussion

The unique fault behaviors of PVPPs further aggravate the adverse effects of fault resistance on distance relay on the PVPP side, and thereby distance relay on the PVPP side is prone to incorrect operations, potentially deteriorating the stability of the power grid. To tackle this issue, this article proposes adaptive mho characteristic-based distance protection to protect the lines emanating from PVPPs. The simulation results confirm that the proposed scheme can distinguish between internal and external faults under various circumstances, and performs better than prior-art schemes. The main reasons that the proposed scheme is chosen and expected to perform better than its prior-art schemes are as follows.

1) The adverse effects caused by the fault resistance are fully considered and eliminated.
2) The unique fault behaviors of PVPPs are considered in this article, so the proposed protection scheme is applicable to the lines emanating from PVPPs.
3) The operation zone of the proposed scheme changes adaptively to adapt to the change in additional impedance. The additional impedance is related to the fault resistance, the output current of PVPP, and the fault current. Therefore, the proposed scheme offers satisfactory tolerance against fault resistance and excellent adaptability to different grid codes, which has been verified in Section IV. In contrast, the majority of prior-art schemes were designed without considering the adaptability to different grid codes.
4) Compared with prior-art schemes, the proposed scheme has some advantages. The prior-art schemes are compared with the proposed scheme from five aspects in Section IV-D. The proposed scheme has the advantages of satisfactory robustness against fault resistance, excellent adaptability to different grid codes, the ability to identify and indicate the fault direction, and no requirements of communication channel and upgrading the software of converter. The comparison results confirm that the proposed scheme is superior to prior-art schemes, regardless of performance or hardware/software cost.

VI. Conclusion

This article proposes a novel distance protection scheme based on adaptive mho characteristic for the transmission lines emanating from the PVPPs. The operation zone of adaptive mho characteristic can adaptively adjust to avoid failure in operation and undesirable operation of distance relay. Some conclusions are as follows.

1) Distance relay with conventional mho or quadrilateral characteristic has a high probability of misidentifying the internal and external faults. By contrast, distance relay with the proposed adaptive mho characteristic can correctly identify the internal and external faults occurring in the lines emanating from the PVPPs.
2) The proposed protection scheme exhibits a superior performance under different fault locations. Besides the identification of internal and external faults, it can identify and indicate the fault direction.
3) The proposed protection scheme offers an excellent robustness against the fault resistance. Furthermore, it exhibits an excellent adaptability to different grid codes.

References

[1] Y. S. Perdana, S. M. Muyeen, A. Al-Durra, H. K. Morales-Paredes, and M. G. Simoes, "Direct connection of supercapacitor–battery hybrid storage system to the grid-tied photovoltaic system," *IEEE Trans. Sustain. Energy*, vol. 10, no. 3, pp. 1370–1379, Jul. 2019.

[2] P. P. Chao *et al.*, "A unified modeling method of photovoltaic generation systems under balanced and unbalanced voltage dips," *IEEE Trans. Sustain. Energy*, vol. 10, no. 4, pp. 1764–1774, Oct. 2019.

[3] H. M. Hasanien, "An adaptive control strategy for low voltage ride through capability enhancement of grid-connected photovoltaic power plants," *IEEE Trans. Power Syst.*, vol. 31, no. 4, pp. 3230–3237, Jul. 2016.

[4] K. Jia, C. J. Gu, Z. W. Xuan, L. Li, and Y. Lin, "Fault characteristics analysis and line protection design within a large-scale photovoltaic power plant," *IEEE Trans. Smart Grid*, vol. 9, no. 5, pp. 4099–4108, Sep. 2018.

[5] Z. K. Shuai, C. Shen, X. Yin, X. Liu, and Z. J. Shen, "Fault analysis of inverter-interfaced distributed generators with different control schemes," *IEEE Trans. Power Del.*, vol. 33, no. 3, pp. 1223–1235, Jun. 2018.

[6] Z. Xu, S. Jiang, Q. Yang, and T. Bi, "Ground distance relaying algorithm for high resistance fault," *IET Gener., Transmiss. Distrib.*, vol. 4, no. 1, pp. 27–35, Jan. 2010.

[7] Z. Xu, S. Jiang, and L. Ran, "Phase distance relaying algorithm for unbalanced inter-phase faults," *IET Gener., Transmiss. Distrib.*, vol. 4, no. 12, pp. 1326–1333, Dec. 2010.

[8] Z. Xu, G. Xu, L. Ran, S. Yu, and Q. Yang, "A new fault-impedance algorithm for distance relaying on a transmission line," *IEEE Trans. Power Del.*, vol. 25, no. 3, pp. 1384–1392, Jul. 2010.

[9] Y. Liang, Z. Lu, W. Li, W. Zha, and Y. Huo, "A novel fault impedance calculation method for distance protection against fault resistance," *IEEE Trans. Power Del.*, vol. 35, no. 1, pp. 396–407, Feb. 2020.

[10] V. H. Makwana and B. R. Bhalja, "A new digital distance relaying scheme for compensation of high-resistance faults on transmission line," *IEEE Trans. Power Del.*, vol. 27, no. 4, pp. 2133–2140, Oct. 2012.

[11] J. Ma, W. Ma, Y. Qiu, and J. Thorp, "An adaptive distance protection scheme based on the voltage drop equation," *IEEE Trans. Power Del.*, vol. 30, no. 4, pp. 1931–1940, Aug. 2015.

[12] J. Ma, X. Xiang, P. Li, Z. Deng, and J. S. Thorp, "Adaptive distance protection scheme with quadrilateral characteristic for extremely high-voltage/ultra-high-voltage transmission line," *IET Gener., Transmiss. Distrib.*, vol. 11, no. 7, pp. 1624–1633, Jun. 2017.

[13] Y. Liang, W. Li, Z. Lu, G. Xu, and C. Wang, "A new distance protection scheme based on improved virtual measured voltage," *IEEE Trans. Power Del.*, vol. 35, no. 2, pp. 774–786, Apr. 2020.

[14] A. D. Filomena, R. H. Salim, M. Resener, and A. S. Bretas, "Ground distance relaying with fault-resistance compensation for unbalanced systems," *IEEE Trans. Power Del.*, vol. 23, no. 3, pp. 1319–1326, Jul. 2008.

[15] M. A. Azzouz, A. Hooshyar, and E. F. El-Saadany, "Resilience enhancement of microgrids with inverter-interfaced DGs by enabling faulty phase selection," *IEEE Trans. Smart Grid*, vol. 9, no. 6, pp. 6578–6589, Nov. 2018.
[16] Y. Chen, M. Wen, X. G. Yin, Y. J. Cai, and J. C. Zheng, "Distance protection for transmission lines of DFIG-based wind power integration system," *Int. J. Elect. Power Energy Syst.*, vol. 100, pp. 438–448, Mar. 2018.
[17] A. Ghorbani, H. Mehrjerdi, and N. A. Al-Emadi, "Distance-differential protection of transmission lines connected to wind farms," *Int. J. Elect. Power Energy Syst.*, vol. 89, pp. 11–18, Jan. 2017.
[18] S. Chen, N. Tai, C. Fan, J. Liu, and S. Hong, "Adaptive distance protection for grounded fault of lines connected with doubly-fed induction generators," *IET Gener., Transmiss. Distrib.*, vol. 11, no. 6, pp. 1513–1520, Feb. 2017.
[19] A. Hooshyar, M. A. Azzouz, and E. F. El-Saadany, "Distance protection of lines connected to induction generator-based wind farms during balanced faults," *IEEE Trans. Sustain. Energy*, vol. 5, no. 4, pp. 1193–1203, Oct. 2014.
[20] K. Jia, Y. B. Li, Y. Fang, L. M. Zheng, T. S. Bi, and Q. X. Yang, "Transient current similarity based protection for wind farm transmission lines," *Appl. Energy*, vol. 225, pp. 42–51, May 2018.
[21] J. D. Jia, G. Y. Yang, A. H. Nielsen, and P. Rønne-Hansen, "Impact of VSC control strategies and incorporation of synchronous condensers on distance protection under unbalanced faults," *IEEE Trans. Ind. Electron.*, vol. 66, no. 2, pp. 1108–1118, Feb. 2019.
[22] A. Hooshyar, M. A. Azzouz, and E. F. El-Saadany, "Distance protection of lines emanating from full-scale converter-interfaced renewable energy power plants—Part I: Problem statement," *IEEE Trans. Power Del.*, vol. 30, no. 4, pp. 1770–1780, Aug. 2015.
[23] A. Hooshyar, M. A. Azzouz, and E. F. El-Saadany, "Distance protection of lines emanating from full-scale converter-interfaced renewable energy power Plants—Part II: Solution description and evaluation," *IEEE Trans. Power Del.*, vol. 30, no. 4, pp. 1781–1791, Aug. 2015.
[24] Y. Fang, K. Jia, Z. Yang, Y. Li, and T. S. Bi, "Impact of inverter-interfaced renewable energy generators on distance protection and an improved scheme," *IEEE Trans. Ind. Electron.*, vol. 66, no. 9, pp. 7078–7088, Sep. 2019.
[25] K. Jia, J. F. Chen, Z. W. Xuan, C. B. Wang, and T. S. Bi, "Active protection for photovoltaic DC-boosting integration system during FRT," *IET Gener., Transmiss. Distrib.*, vol. 13, no. 18, pp. 4081–4088, Sep. 2019.
[26] I. Hiskens, "IEEE PES task force on benchmark systems for stability controls," Tech. Rep., Nov. 2013. [Online]. Available: http://www.sel.eesc.usp.br/ieee/
[27] Manitoba Hydro International Ltd., "IEEE 39 bus system," IEEE 39 Bus Technical Note, May 2018. [Online]. Available: https://hvdc.ca/knowledge-base/read,article/28/ieee-39-bus-system/v:
[28] "Technical requirement for connecting photovoltaic power station to power system," China Standard GB/T 19964—2012, 2012.
[29] F. Zhang and L. H. Mu, "A fault detection method of microgrids with grid-connected inverter interfaced distributed generators based on the PQ control strategy," *IEEE Trans. Smart Grid*, vol. 10, no. 5, pp. 4816–4826, Sep. 2019.

Yingyu Liang (Member, IEEE) received the B.S. degree from Northeast Electric Power University, Jilin, China, and the Ph.D. degree in power system and its automation from North China Electric Power University, Beijing, China, in 2016.

He is currently an Associate Professor with the China University of Mining and Technology (Beijing), Beijing, China. His research interests include power system protection and control of renewable energy systems and VSC-HVdc.

Wulin Li was born in Shanxi, China. He received the B.S. degree from Datong University, Datong, China, in 2017. He is currently working toward the M.Sc. degree in electrical engineering with the China University of Mining and Technology (Beijing), Beijing, China.

His research interests include power system protection and control of renewable energy systems.

Wenting Zha received the B.S. and the Ph.D. degrees from Southeast University, Nanjing, China, in 2011 and 2016, respectively.

She is currently a Lecturer with the China University of Mining and Technology (Beijing), Beijing, China. Her research interests include the application of nonlinear control and artificial intelligence in power systems.